

# Effect of manganese doping on Li-ion intercalation properties of V<sub>2</sub>O<sub>5</sub> films

D. M. Yu,<sup>ab</sup> S. T. Zhang,<sup>ab</sup> D. W. Liu,<sup>a</sup> X. Y. Zhou,<sup>a</sup> S. H. Xie,<sup>cd</sup> Q. F. Zhang,<sup>a</sup> Y. Y. Liu<sup>a</sup> and G. Z. Cao<sup>\*a</sup>

Received 28th April 2010, Accepted 19th September 2010

DOI: 10.1039/c0jm01252a

Mn-doped V<sub>2</sub>O<sub>5</sub> has been prepared by sol-gel processing with H<sub>2</sub>O<sub>2</sub> and V<sub>2</sub>O<sub>5</sub> as precursors with Mn<sup>2+</sup> added directly during sol preparation. Stable and homogeneous Mn-doped vanadium oxide sol was obtained and the films were fabricated by dip-coating, drying at ambient, and then annealing at 250 °C in air for 3 h. X-Ray diffraction (XRD), X-ray photoelectron spectroscopy (XPS), atomic force microscopy (AFM), and electrochemical analyses have been employed to characterize and analyze the crystal- and microstructures, surface morphology and Li-ion intercalation properties of both Mn-doped and undoped V<sub>2</sub>O<sub>5</sub> films. Mn-doped V<sub>2</sub>O<sub>5</sub> films exhibit excellent cyclic stability with a fading rate of less than 0.06% per cycle, significantly better than that of the pure V<sub>2</sub>O<sub>5</sub> films (0.8% per cycle). Mn-doped V<sub>2</sub>O<sub>5</sub> films have demonstrated a large discharge capacity of ~283mAh/g with a current density of 68 mA/g, again much higher than 237 mAh/g of V<sub>2</sub>O<sub>5</sub> films. A possible explanation for such significant enhancement in lithium ion intercalation capacity, cyclic stability, and rate performance of Mn-doped V<sub>2</sub>O<sub>5</sub> films has been discussed.

## 1. Introduction

In recent years, the increase in the demand for rechargeable lithium-ion batteries has experienced a huge rise, and the study of suitable electrode materials has been focused on finding alternative cathodic materials to replace the commercialized lithium cobalt oxide electrode, which has the bad traits of high cost and toxicity.<sup>1,2</sup> There are two categories of cathodic materials for rechargeable lithium-ion batteries.<sup>3</sup> One is layered compounds with an anion close-packed lattice and the inherent advantage of higher energy density owing to their structural characteristic. LiTiS<sub>2</sub>, LiCoO<sub>2</sub>, LiNi<sub>1-x</sub>Co<sub>x</sub>O<sub>2</sub>, and LiNi<sub>x</sub>Mn<sub>x</sub>Co<sub>1-2x</sub>O<sub>2</sub> all belong to this group. The other one, such as vanadium oxides, the tunnel compounds of manganese oxides, and transition metal phosphates (e.g. the olivine LiFePO<sub>4</sub>), is the class of materials with more opened structures and the advantages of better safety and lower cost compared to the first group.

Since the reversible electrochemical lithium ion intercalation in V<sub>2</sub>O<sub>5</sub> was first reported in 1976 by Whittingham *et al.*,<sup>4</sup> vanadium pentoxide has been intensively investigated as a cathode material for rechargeable lithium-ion batteries because of its low cost, abundance, easy synthesis, and high energy density. It is a typical intercalation compound with a layered crystal structure, with a large variety of atomic and molecular species that can be reversibly intercalated and extracted between the layers. However, the development of rechargeable lithium-ion batteries with vanadium pentoxide as a cathode has been limited for its

poor structural stability, low electronic conductivity and ionic conductivity,<sup>5,6</sup> and slow electrochemical kinetics.

A lot of recent research has been focused on the synthesis and fabrication of nanostructured vanadium oxides to mitigate the slow electrochemical kinetics with high specific surface area and short diffusion distance.<sup>7</sup> For example, single-crystal V<sub>2</sub>O<sub>5</sub> nanorod arrays demonstrated much improved electrochemical Li-ion intercalation properties.<sup>8-10</sup> Such improvement has been attributed to the long axis (growth direction) of the single-crystal nanorod arrays parallel to the interlayer of V<sub>2</sub>O<sub>5</sub>, and thus providing shorter and simpler diffusion paths for lithium ions and allowing the most freedom for dimension change accompanying the lithium ion intercalation and extraction. Similar enhancement has been found in platelet- and fibrillar-structured V<sub>2</sub>O<sub>5</sub> films; however, some nanostructured films suffer from poor cyclic stability.<sup>11,12</sup> The cyclic stability could be improved when nanostructures are appropriately designed and fabricated.<sup>13,14</sup>

Doping transition metal ions has been studied for improved lithium ion intercalation properties. For example, doping of Ag and Cu in vanadium oxides<sup>15-17</sup> has been reported to result in much improved electrochemical properties of V<sub>2</sub>O<sub>5</sub>. Coustier *et al.*<sup>15</sup> found that the electronic conductivity of V<sub>2</sub>O<sub>5</sub> films was increased by 2 to 3 orders of magnitude owing to addition of Ag, while Cu-doped V<sub>2</sub>O<sub>5</sub> exhibited promising electrochemical performance.<sup>18</sup> Park<sup>19</sup> prepared Mn<sub>x</sub>V<sub>2</sub>O<sub>5</sub> by a multi-step approach combining sol-gel processing and ion exchange treatment and demonstrated higher intercalation capacity and discharge voltage, both of which increased with the increase of manganese doping concentration. However, these Mn<sub>x</sub>V<sub>2</sub>O<sub>5</sub> gels need to be aged for at least a month at 30 °C in order to ensure homogenization before being tested, while their discharge capacity is lower and the maximum is less than 150mAh/g. In this paper, we report the preparation and characterization of Mn-doped V<sub>2</sub>O<sub>5</sub> films by a simple sol-gel process, which delivers higher lithium ion intercalation capacity and much improved cyclic stability in comparison with pure V<sub>2</sub>O<sub>5</sub>. The crystal and microstructures,

<sup>a</sup>Department of Materials Science and Engineering, University of Washington, Seattle, WA, 98195, USA

<sup>b</sup>College of Chemistry and Chemical Engineering, Chongqing University, Chongqing, 400044, P. R. China

<sup>c</sup>Department of Mechanical Engineering, University of Washington, Seattle, WA, 98195, USA

<sup>d</sup>Faculty of Materials, Optoelectronics and Physics, Xiangtan University, Xiangtan, Hunan, 411105, P. R. China

surface morphology, and lithium ion intercalation properties of Mn-doped  $V_2O_5$  films were studied.

## 2. Experimental

Vanadium oxide sol was prepared using the method reported by Fontenot *et al.*<sup>20</sup> 0.136g  $V_2O_5$  powder (Alfa Aesar) was dissolved in 2.0 ml de-ionized water and 0.603 ml 30%  $H_2O_2$  solution at room temperature. The suspension was stirred vigorously until  $V_2O_5$  dissolved totally and a clear dark red solution was obtained. The solution was then sonicated to get a yellow-brown gel, which was dispersed into 150ml de-ionized water with primary vanadium species in the colloidal dispersion nanoparticles of hydrated vanadium oxide, a molar concentration of 0.005 mol/L and pH of  $\sim 3.0$ . To obtain Mn-doped vanadium oxide sol, the appropriate amount ( $\sim 1.67\%$ ) of  $Mn(Ac)_2 \cdot 4H_2O$  (Alfa Aesar) first was added into  $V_2O_5$  powder and mixed, and then, dissolved in de-ionized water and 30%  $H_2O_2$  solution, following the same procedure for the preparation of vanadium oxide sol. Unlike Park's method,<sup>19</sup> the preparation of Mn-doped  $V_2O_5$  sol and film did not require aging as  $Mn(Ac)_2 \cdot 4H_2O$  was readily dissolved and dispersed uniformly in the solution. Mn-doped  $V_2O_5$  films and  $V_2O_5$  films were prepared by spreading 50 $\mu$ l of the sols onto fluorine-doped tin oxide (FTO) glass substrates. After drying at ambient condition for 24 h, the films were annealed at 250 °C in air for 3 h.

The surface morphology, crystallinity and valence state of both Mn-doped  $V_2O_5$  films and  $V_2O_5$  films were characterized by means of atomic force microscopy (AFM, Asylum Research MFP-3D), X-ray diffraction (XRD, Philips 1820 X-ray diffractometer) and X-Ray photoelectron spectroscopy. All XPS spectra were taken on a Kratos Axis-Ultra DLD spectrometer. This instrument has a monochromatized Al  $K\alpha$  X-ray source and a low energy electron flood gun for charge neutralization. X-Ray spot size for these acquisitions was on the order of 300x700  $\mu$ m (Kratos 'Hybrid' mode). Pressure in the analytical chamber during spectral acquisition was less than  $5 \times 10^{-9}$  Torr. Pass energy for survey spectra was 80 eV and the pass energy for the high resolution scans was 20 eV. The take-off angle (the angle between the sample normal and the input axis of the energy analyzer) was 0° (0 degree take-off angle  $\cong$  100 Å sampling depth).

The electrochemical properties of Mn-doped  $V_2O_5$  films and  $V_2O_5$  films were studied using a standard three-electrode system, with 1M  $LiClO_4$  in propylene carbonate as the electrolyte, a Pt flake as the counter electrode, and Ag/AgCl as the reference electrode. Cyclic voltammetric (CV) tests were carried out between 0.5 and  $-1.4$  V ( $\sim 3.6$  V– $1.7$  V vs.  $Li^+/Li$ ) with a scan rate of 10 mV/s, while the charge-discharge properties of these films were investigated by chronopotentiometric (CP) measurements in the voltage from 0.5 V to  $-1.4$  V with various current density. Both the CVs and CPs were performed by using an electrochemical analyzer (CH Instruments, Model 605 B).

## 3. Results and discussion

Fig. 1 is the XRD patterns of Mn-doped  $V_2O_5$  films and  $V_2O_5$  films annealed at 250 °C in air for 3 h. Both samples have broad peaks centered around  $2\theta = 8^\circ$ , indicative of a predominant

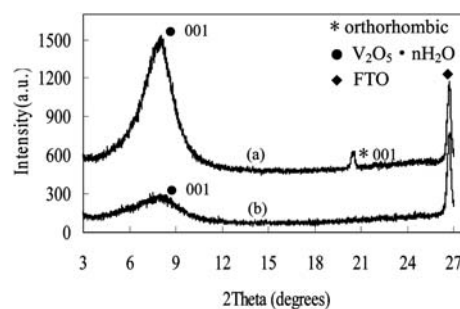
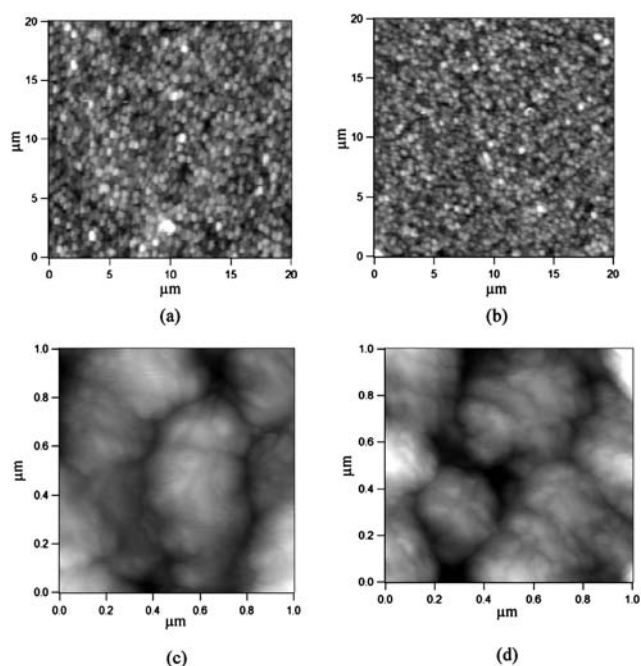


Fig. 1 XRD patterns of (a)  $V_2O_5$  films and (b) Mn-doped  $V_2O_5$  films.

amorphous nature and similar to those of  $V_2O_5 \cdot nH_2O$  xerogels reported in the literature,<sup>21,22</sup> suggesting both samples are hydrous vanadium pentoxide. No secondary or parasitic phase was detectable. However, both films do consist of a small amount of or partial crystalline phases as evidenced by the presence of characteristic diffraction (001) peak. Although both films have similar thicknesses, due to the same amount of solid applied for the film fabrication and as evidenced by the similar height of the FTO diffraction peak, the (001) diffraction peak of Mn-doped hydrous  $V_2O_5$  films possesses broader full width at half-maximum than that of hydrous  $V_2O_5$  films with a position shift towards lower angle. For interlayer spacing of hydrous  $V_2O_5$  films, the interlayer spacing was estimated using the Scherrer equation,<sup>23,24</sup> and found to be  $\sim 11\text{Å}$ , close to that of hydrous  $V_2O_5$  with 0.3 water molecules.<sup>22</sup> Mn-doped sample was found to have an interlayer distance of  $\sim 11.3\text{Å}$ , slightly larger, possibly due to the incorporation of larger manganese ion ( $Mn^{2+}$ : 83pm with CN = 6 versus  $V^{5+}$ : 54 pm<sup>25</sup>) into the lattice of hydrous vanadium oxide. The impact of the slight increase in the cation size may be compensated by the formation of oxygen vacancies, which generally lead to a relatively open structure with a reduced lattice constant.<sup>26</sup> The grain size of Mn-doped  $V_2O_5$  films was found to be  $\sim 1.5$  nm, smaller than  $\sim 3.5$  nm in  $V_2O_5$  films. In addition, the Mn doping has resulted in the suppression of the formation of orthorhombic  $V_2O_5$ , which was found to coexist in the undoped  $V_2O_5$  sample, indicating the phase transition was inhibited by the introduction of manganese ions into hydrous vanadium structure. Similar observations have also been reported for Cu, Cr doped  $V_2O_5$  and PEDOT- $V_2O_5$  hybrid materials.<sup>27–29</sup>

Fig. 2 is the top view AFM images of Mn-doped  $V_2O_5$  films and  $V_2O_5$  films annealed at 250 °C in air for 3 h. It is clear that both films are coherent and homogeneous, consisting of sub-microsized particles. The film thickness of both samples is  $\sim 250$  nm determined by AFM. It is also found in Fig. 2 (c) and (d) that these submicrosized particles are aggregates made of much smaller nanoparticles. The particle size estimated from the XRD patterns using the Scherrer equation<sup>23</sup> was found to be  $\sim 1.5$  nm in Mn-doped  $V_2O_5$  films and  $\sim 3.5$  nm undoped  $V_2O_5$  films, respectively. Although transmission electron microscopy (TEM) images would provide direct evidence of the particle size, it was very difficult to prepare the samples and get quality images to show the aggregation of nanometer sized particles.

X-Ray photoelectron spectroscopy (XPS) analyses show both  $V^{4+}$  ions and  $V^{5+}$  ions coexist in Mn-doped  $V_2O_5$  sample, and the  $V^{4+}/V^{5+}$  ratio is  $\sim 0.22$ , suggesting the formation of low valence state vanadium. From the literature<sup>25</sup>

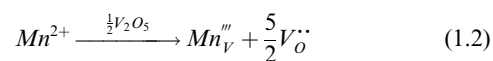


**Fig. 2** AFM images of (a) and (c) Mn-doped  $V_2O_5$  films, and of (b) and (d) undoped  $V_2O_5$  films.

$$E^{\theta}(VO_2^+/VO^{2+}) = 0.991 V, E^{\theta}(Mn^{3+}/Mn^{2+}) = 1.542 V \quad (1.1)$$

Because the potential of  $E^{\theta}(VO_2^+/VO^{2+})$  is not larger than that of  $E^{\theta}(Mn^{3+}/Mn^{2+})$ , it is impossible for  $V^{4+}$  and  $Mn^{3+}$  to coexist in the structure of vanadium oxide, and the valence state of manganese would remain divalence in Mn-doped  $V_2O_5$ . According to the result of XPS investigation, it can be determined that the formula of Mn-doped  $V_2O_5$  is  $(Mn, V)_2O_{4.74}(V_{\delta})_{0.26}$ . Based on the similarity in ionic radii between  $Mn^{2+}$  and

$V^{5+}$  in the same coordination number,<sup>26</sup> it may be presumed that manganese ions will enter the  $V_2O_5$  crystals and substitute partially for vanadium. So the defect chemical reaction is



where  $V_{\delta}^{''}$  represents oxygen vacancies with a doubly positive charge relative to the perfect lattice, because there is the absence of an  $O^{2-}$  ion, while  $Mn_V^{'''}$  is a manganese substitutional defect. The presence of oxygen vacancies results in the formation of more open structure and easy access for lithium ion intercalation and diffusion. In addition, they may serve as possible nucleation centers for phase transformation during the lithium ion insertion and extraction processes.<sup>30</sup> Moreover, the conductivity of the film can be enhanced owing to the presence of lower valence vanadium ions and associated oxygen vacancies.<sup>31</sup>

Fig. 3(a) is a typical CV curve of  $V_2O_5$  films in the potential region of 0.5 to  $-1.4V$  vs.  $Ag/Ag^+$ , with a scan rate of 10 mV/s. Three reduction peaks at  $-0.32 V$ ,  $-0.63 V$  and  $-1.15 V$  correspond to the phase transitions to the  $\delta$ ,  $\beta$  and  $\gamma$  phases, respectively, accompanying the  $Li^+$  intercalation, while more than three peaks are observed in the oxidation process. It is likely to suggest that there is permanent phase transition in the structure of  $V_2O_5$  films during the first cycles, as reported previously in the literature.<sup>32,33</sup> Fig. 3(b) shows the CV curve of Mn-doped  $V_2O_5$  films, exhibiting two pairs of well-defined redox peaks in the first cycle, located at  $-0.45 V/-0.78 V$  and  $-0.84 V/-1.11 V$ , respectively. This implies that the number of phase transition decreases and the irreversible phases transition observed in  $V_2O_5$  films are effectively suppressed or eliminated by  $Mn^{2+}$  doping.<sup>28</sup> Fig. 3 (c) and (d) compares the CV curves in the 1st and 10th cycles of Mn-doped and undoped  $V_2O_5$  films. There are a number of noticeable differences, including significant reduction of the current (peak heights) associated with the anodic and cathodic reactions

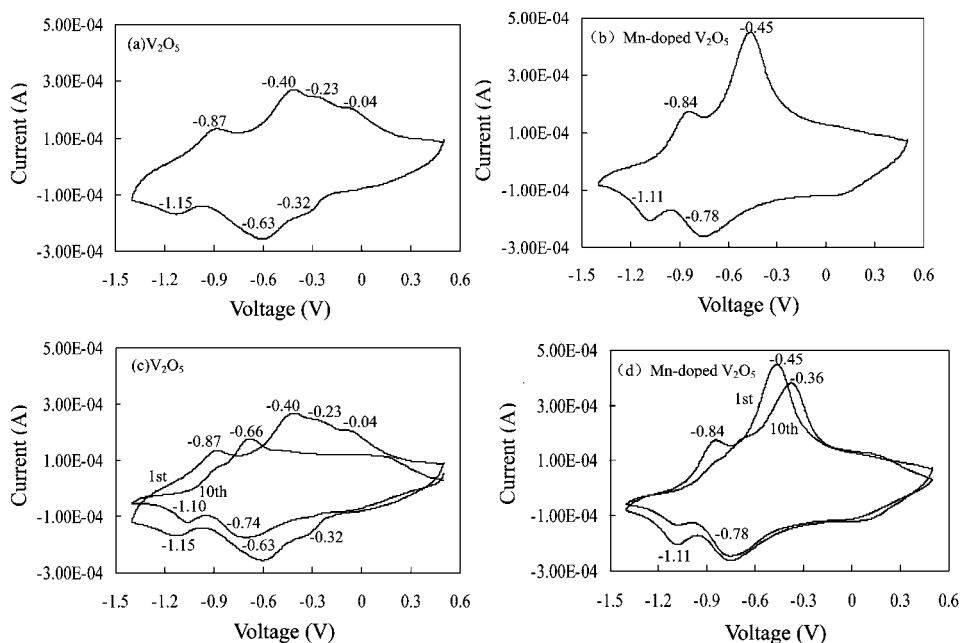


**Fig. 3** Cyclic voltammetry curves of (a) the first cycle of  $V_2O_5$  film, (b) the first cycle of Mn-doped  $V_2O_5$  film, (c) the first and tenth cycles of  $V_2O_5$  film and (d) the first and tenth cycles of Mn-doped  $V_2O_5$  film. The scan rate is 10 mV/s.

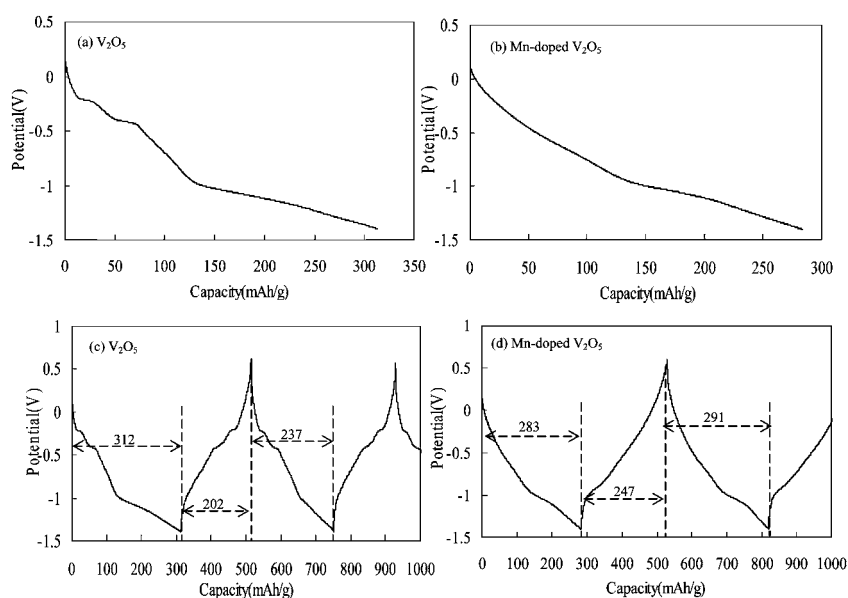
and the shift of peak positions during repetitive cycling between 0.5 and  $-1.4$  V vs.  $\text{Ag}/\text{Ag}^+$  under the same scan rate in Fig. 3 (c), whereas the change of current value and peak position is not remarkable after Mn-doped  $\text{V}_2\text{O}_5$  films is charged/discharged 10 cycles with the same condition as  $\text{V}_2\text{O}_5$  films (shown in Fig. 3(d)), suggesting the improvement of electrochemical stability by the addition of  $\text{Mn}^{2+}$ . It should be noticed that the pair of redox peaks located at  $-0.84$  V/ $-1.11$  V disappears gradually with the repetitive cycling of doped-Mn  $\text{V}_2\text{O}_5$  films, and it is beneficial to increase cycling stability of the electrode material. Similar observation is found in the cycling of undoped  $\text{V}_2\text{O}_5$  films, too. It explains why the degeneration of electrochemical properties of  $\text{V}_2\text{O}_5$  film may become slow during the cycles. However, in comparison with pure  $\text{V}_2\text{O}_5$  films, cathodic peaks positions of Mn-doped  $\text{V}_2\text{O}_5$  films almost do not shift after 10 cycles, showing better stability of the operation voltage in lithium ion batteries with Mn-doped  $\text{V}_2\text{O}_5$  cathode. Moreover, the close two pairs of well-defined redox peaks also reflect the increased lithium-ion diffusion kinetics of the electrode material owing to doping manganese.<sup>14</sup>

Fig. 4 shows the chronopotentiometric (CP) curves of Mn-doped  $\text{V}_2\text{O}_5$  films and undoped  $\text{V}_2\text{O}_5$  films under current density of 68 mA/g and potential ranging from 0.5 to  $-1.4$  V vs.  $\text{Ag}/\text{Ag}^+$ . It demonstrates that the intercalation/de-intercalation behavior of  $\text{V}_2\text{O}_5$  films is affected obviously by the incorporation of divalent manganese ions. The CP curve of  $\text{V}_2\text{O}_5$  films possesses a more staircase-type shape, resulting from possible better defined phase transitions during cathodic and anodic processes, while the CP curve of Mn-doped  $\text{V}_2\text{O}_5$  films lacks of obvious staircase-like shape, suggesting less defined phase transition associated with lithium-ion intercalation and de-intercalation, due to much poor crystallinity or amorphous-like nature of Mn-doped  $\text{V}_2\text{O}_5$  films as revealed by XRD patterns (shown in Fig. 1). It is also noticed that pure  $\text{V}_2\text{O}_5$  film delivers a high initial discharge capacity of 313 mAh/g, but a charge capacity of only

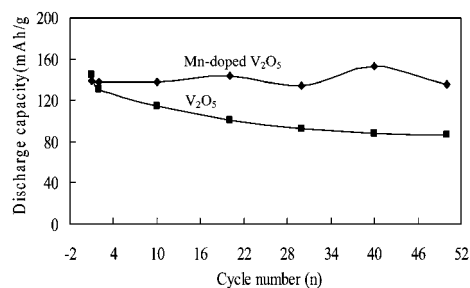
202 mAh/g, with an irreversible capacity loss of 111 mAh/g, and consequently, the discharge capacity in the second cycle reduces to 237 mAh/g, corresponding to a discharge capacity loss of 24%. Mn-doped  $\text{V}_2\text{O}_5$  films demonstrates an initial discharge capacity of 283 mAh/g, with a corresponding charge capacity of 247 mAh/g, 36 mAh/g lower than the discharge capacity, and the second discharge capacity is 291 mAh/g, a slightly higher than initial discharge capacity. The improvement of intercalation/de-intercalation behavior of vanadium pentoxide could be ascribed to the presence of oxygen vacancies, the decrease of the number of phase transition and the removal of the irreversible phase transition due to the incorporation of manganese ions.

Fig. 5 compares the cyclic performance of  $\text{V}_2\text{O}_5$  films and Mn-doped  $\text{V}_2\text{O}_5$  films at a high current density of 680mA/g. The  $\text{V}_2\text{O}_5$  films exhibit a drastic capacity fade, from the initial 145mAh/g at the 1st cycle to 131mAh/g, 10% loss at the 2nd cycle, and then it further decreases to 86mAh/g at the 50th cycle, a 40% loss of the initial discharge capacity. In contrast, Mn-doped  $\text{V}_2\text{O}_5$  films start with the discharge capacity of 138mAh/g, and retains a discharge capacity of 135mAh/g at the 50th cycle, with less than 3.0% loss.

The cyclic stability of Mn-doped  $\text{V}_2\text{O}_5$  films was studied further with interrupted cyclic testing. Fig. 6 summarizes the cyclic performance of Mn-doped  $\text{V}_2\text{O}_5$  films underwent 6 times interruption and repetitive charge/discharge cycles, that is, the same sample was charged/discharged over again after finished previous continuous charge/discharges. More specifically, the sample was taken out the cell system and laid in air after it was charge/discharged 5 cycles in the first continuous charge/discharge test. Then this same sample was charge/discharged continuously 50 cycles again, following the same procedure, the cycle number of the third, fourth, the fifth and the sixth continuous charge/discharge is 50, 15, 30 and 250, respectively, and the total cycle number is 400. It is found that regardless the repeated interruptions over 400 cyclic charge/discharge tests, the discharge capacity of Mn-doped



**Fig. 4** Chronopotentiometric curves of (a) the initial discharge of  $\text{V}_2\text{O}_5$ , (b) the initial discharge of Mn-doped  $\text{V}_2\text{O}_5$ , (c) the first charge-discharge of  $\text{V}_2\text{O}_5$  and (d) the first charge-discharge of Mn-doped  $\text{V}_2\text{O}_5$  under a current density of 68 mA/g, potential ranging from 0.5 to  $-1.4$  V vs.  $\text{Ag}/\text{Ag}^+$ .



**Fig. 5** The discharge capacity of V<sub>2</sub>O<sub>5</sub> films and Mn-doped V<sub>2</sub>O<sub>5</sub> films, at a current density of 680 mA/g, potential ranging from 0.5 to -1.4 V vs. Ag/Ag<sup>+</sup>.

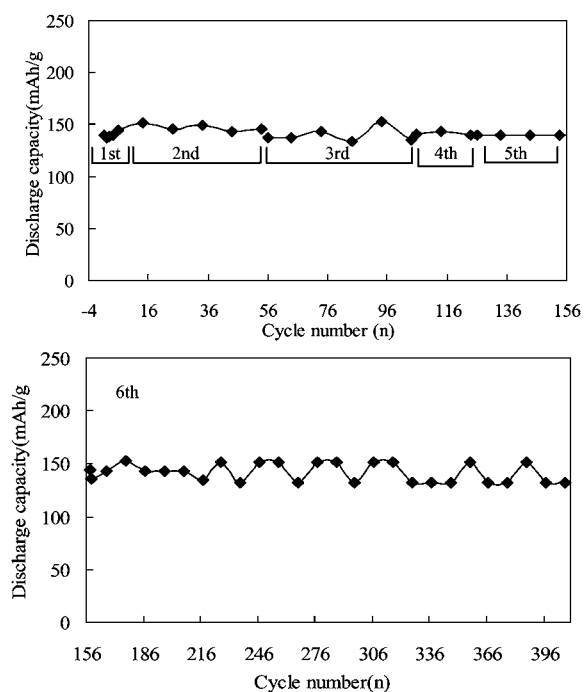


**Fig. 6** Cycling performance of Mn-doped V<sub>2</sub>O<sub>5</sub> films under interrupted charge/discharge cycles, at a current density of 680 mA/g, potential ranging from 0.5 to -1.4 V vs. Ag/Ag<sup>+</sup>.

V<sub>2</sub>O<sub>5</sub> films remains fairly constant and only a very small loss of less than 5.0% at the 400th cycle is found. Such an excellent electrochemical stability of Mn-doped V<sub>2</sub>O<sub>5</sub> films could be attributed to poor crystallinity or amorphous-like nature and the presence of oxygen vacancies. The amorphous film would not possess a well defined phase transition as evidenced with lack of charge/discharge plateaus in CP curves (Fig. 4b and 4d) and, thus, stress or strain resulted from the phase transition accompanied to lithium ion intercalation and extraction would be dispersed through the charge/discharge process. The presence of oxygen vacancies and manganese ions might serve as nucleation centers in phase transformation that occurred during lithium ions intercalation/de-intercalation. For this reason, the phase transformation process is much easier and dimensions change is also mitigated during the charge/discharge process of Mn-doped V<sub>2</sub>O<sub>5</sub> films.

Fig. 6 also reveals that the lithium-ion intercalation capacity of Mn-doped V<sub>2</sub>O<sub>5</sub> films fluctuates noticeably, particularly at the

cycles larger than 150. The exact cause for such a fluctuation is not known to us at the moment. However, the cautions were taken during the measurements. The possible contamination in electrolyte, for example, by oxygen or moisture, can be excluded: (1) the cyclic tests for both Mn-doped and undoped V<sub>2</sub>O<sub>5</sub> films were done under the same conditions and no fluctuation was found in undoped V<sub>2</sub>O<sub>5</sub> films, (2) the same measurements have been used in our lab for other electrodes and no such fluctuation was found, and (3) we did compare the measurements on the same electrodes in our lab using the method described in this paper and at Pacific Northwest National Labs using the standard coin-cell method, and found no noticeable difference, though our measurement method admittedly looks much simpler and rudimentary. However, the fluctuation in discharge capacity in vanadium pentoxide electrodes with doping has also reported in literature, although in a less degree.<sup>15,19,34,35</sup> More detailed work is planned to obtain a better understanding on the relationship between point defects and such capacity fluctuation.

Fig. 7 presents the lithium ion intercalation capacity as a function of current density for V<sub>2</sub>O<sub>5</sub> films and Mn-doped V<sub>2</sub>O<sub>5</sub> films. For both films, the discharge capacity decreases with the increase of current density as observed in all electroactive materials for lithium ion intercalation and extraction. In the entire range of current density studied in this research, the discharge capacity of Mn-doped V<sub>2</sub>O<sub>5</sub> films is always higher than that of undoped V<sub>2</sub>O<sub>5</sub> films measured under identical conditions including the same current density. The experimental results have demonstrated that the Mn-doped V<sub>2</sub>O<sub>5</sub> films possess larger discharge capacity with better kinetics as well as much improved cyclic stability than that of undoped V<sub>2</sub>O<sub>5</sub> films. Although the exact mechanism(s) for such an improvement is unknown, the much reduced crystallinity and the presence of oxygen vacancies resulted from the Mn doping could be likely the causes for such change and improvement in electrochemical properties of Mn-doped V<sub>2</sub>O<sub>5</sub> films. The literature<sup>26,36</sup> suggests that when V<sup>5+</sup> ions are partially replaced by doping metal ions, [MO<sub>6</sub>] octahedral may form in the framework of V<sub>2</sub>O<sub>5</sub>, introducing the three-dimensional character, which makes the crystal structure stronger in dealing with the deformation of the material structure during Li-ion intercalation and de-intercalation cycling. In addition, the presence of oxygen vacancies may alleviate the stress or strain accompanied to the Li-ion intercalation and de-intercalation process, leading to further improved cyclic stability.

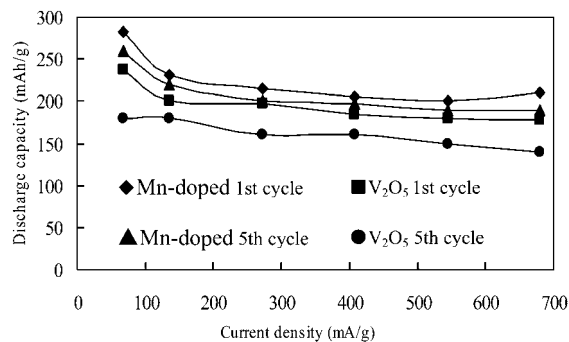


**Fig. 7** Relationship between discharge capacity and current density for V<sub>2</sub>O<sub>5</sub> and Mn-doped V<sub>2</sub>O<sub>5</sub> films, potential ranging from 0.5 to -1.4 V vs. Ag/Ag<sup>+</sup>.

## 4. Conclusions

Mn-doped V<sub>2</sub>O<sub>5</sub> films have been prepared by a simple H<sub>2</sub>O<sub>2</sub>-V<sub>2</sub>O<sub>5</sub> sol-gel process with the direct addition of manganese salt. Mn-doping in V<sub>2</sub>O<sub>5</sub> films results in enhanced discharge capacities with much improved cyclic stability. For example, at a current density of 68 mA/g, Mn-doped V<sub>2</sub>O<sub>5</sub> films exhibit a discharge capacity of ~ 283 mAh/g. Excellent cyclic stability with a fading rate of less than 0.06% per cycle is observed even at a very high current density of 680 mA/g, much better than pure V<sub>2</sub>O<sub>5</sub> films (0.8%). The improved lithium ion intercalation capacity, cyclic stability, and rate performance of Mn-doped V<sub>2</sub>O<sub>5</sub> films could be attributed to the introduction of oxygen vacancies and the formation of [MnO<sub>6</sub>] octahedra due to adding appropriate amount manganese into vanadium pentoxide.

## Acknowledgements

This work was supported in part by National Science Foundation (CMMI 1030048) and Air Force Office of Scientific Research (AFOSR-MURI, FA9550-06-1-0326). D. M. Y. would like to acknowledge the fellowship from the Chinese Scholarship Council.

## References

- 1 A. Manthiram and J. Kim, *Chem. Mater.*, 1998, **10**, 2895.
- 2 J. S. Yang and J. J. Xu, *J. Power Sources*, 2003, **122**, 181.
- 3 Y. Wang and G. Z. Cao, *Adv. Mater.*, 2008, **20**, 2251.
- 4 M. S. Whittingham, *J. Electrochem. Soc.*, 1976, **123**, 315.
- 5 J. X. Wang, C. J. Curtis, D. L. Schulz and J. G. Zhang, *J. Electrochem. Soc.*, 2004, **151**, A1.
- 6 R. Baddour-Hadjean, J. P. Pereira-Ramos, C. Navone and M. Smirnov, *Chem. Mater.*, 2008, **20**, 1916.
- 7 K. Takahashi, S. J. Limmer, Y. Wang and G. Z. Cao, *J. Phys. Chem. B*, 2004, **108**, 9795.
- 8 K. Takahashi, S. J. Limmer, Y. Wang and G. Z. Cao, *Jpn. J. Appl. Phys.*, 2005, **44**, 662.
- 9 K. Takahashi, Y. Wang and G. Z. Cao, *Appl. Phys. Lett.*, 2005, **86**, 053102.
- 10 N. Li, C. J. Patrissi and C. R. Martin, *J. Electrochem. Soc.*, 2000, **147**, 2044.
- 11 K. Lee, Y. Wang and G. Z. Cao, *J. Phys. Chem. B*, 2005, **109**, 16700.
- 12 Y. Wang and G. Z. Cao, *Chem. Mater.*, 2006, **18**, 2787.
- 13 C. Navone, R. Baddour-Hadjean, J. P. Pereira-Ramos and R. Salot, *J. Electrochem. Soc.*, 2005, **152**, A1790.
- 14 D. W. Liu, Y. Y. Liu, B. B. Garcia, Q. F. Zhang, A. Q. Pan, Y. H. Jeong and G. Z. Cao, *J. Mater. Chem.*, 2009, **19**, 8789.
- 15 F. Coustier, S. Passerini and W. H. Smyrl, *Solid State Ionics*, 1997, **100**, 247.
- 16 M. Giorgetti, M. Berrettoni and W. H. Smyrl, *Chem. Mater.*, 2007, **19**, 5991.
- 17 C. Leger, S. Bach, P. Soudan and J.-P. Pereira-Ramos, *Solid State Ionics*, 2005, **176**, 1365.
- 18 Y. J. Wei, C. W. Ryu and K. B. Kim, *J. Alloys Compd.*, 2008, **459**, L13.
- 19 H.-K. Park, *Solid State Ionics*, 2005, **176**, 307.
- 20 C. J. Fontenot, J. W. Wiench, M. Pruski and G. L. Schrader, *J. Phys. Chem. B*, 2000, **104**, 11622.
- 21 V. Petkov, P. N. Trikalitis, S. E. Bozin, L. J. S. Billinge, T. Vogt and G. M. Kanatzidis, *J. Am. Chem. Soc.*, 2002, **124**, 10157.
- 22 Y. Wang, H. M. Shang, T. Chou and G. Z. Cao, *J. Phys. Chem. B*, 2005, **109**, 11361.
- 23 G. Z. Cao, *Nanostructures and Nanomaterials, synthesis Properties and Applications*, Imperial College Press, London, 2004.
- 24 L. S. Birks and H. Friedman, *J. Appl. Phys.*, 1964, **17**, 687.
- 25 D. R. Lide, *Handbook of Chemistry and Physics*, 88th Edition, CRC Press, New York, 2008.
- 26 Y. M. Chiang, D. Birnie, W. D. Kingery, *Physical Ceramics, Principles for Ceramic Science and Engineering*, John Wiley and Sons, Inc. Canada, 1997.
- 27 Y. J. Wei, C. W. Ryu and K. B. Kim, *J. Power Sources*, 2007, **165**, 386.
- 28 S. Y. Zhan, C. Z. Wang, K. Nikolowski, H. Ehrenberg, G. Chen and Y. J. Wei, *Solid State Ionics*, 2002, **105**, 1.
- 29 A. V. Murugan, C.-W. Kwon, G. Campet, B. B. Kale, T. Maddanimath and K. Vijayamohan, *J. Power Sources*, 2007, **165**, 386.
- 30 Y. H. Zhang, P. Xiao, X. Y. Zhou, D. W. Liu, B. B. Garcia and G. Z. Cao, *J. Mater. Chem.*, 2009, **19**, 948.
- 31 Q. H. Wu, A. Thissen, W. Jaegermann and M. Liu, *Appl. Surf. Sci.*, 2004, **236**, 473.
- 32 J. Livage, *Chem. Mater.*, 1991, **3**, 578.
- 33 F. J. Anaissi, G. J. F. Demets and H. E. Toma, *Electrochem. Commun.*, 1999, **1**, 332.
- 34 F. Coustier, J. Hill, B. B. Owens, S. Passerini and W. H. Smyrl, *J. Electrochem. Soc.*, 1999, **146**, 1355.
- 35 S. Zhan, Y. J. Wei, X. F. Bie, C. Z. Wang, F. Du, G. Chen and F. Hu, *J. Alloys Compd.*, 2010, **502**, 92.
- 36 G. Gregoire, N. Baffier, A. K. Harari and J. C. Badot, *J. Mater. Chem.*, 1998, **8**, 2103.